

The Cellulase KORRIGAN Is Part of the Cellulose Synthase Complex^{1[W]}

Thomas Vain^{2,3}, Elizabeth Faris Crowell², H el ene Timpano⁴, Eric Biot, Thierry Desprez, Nasim Mansoori⁵, Luisa M. Trindade, Silv ere Pagant⁶, St ephanie Robert⁴, Herman H ofte, Martine Gonneau, and Samantha Vernhettes*

Institut National de la Recherche Agronomique, Unit e Mixte de Recherche 1318, Institut Jean-Pierre Bourgin, Saclay Plant Sciences, F-78000 Versailles, France (T.V., E.F.C., H.T., E.B., T.D., S.P., S.R., H.H., M.G., S.V.); AgroParisTech, Institut Jean-Pierre Bourgin, F-78000 Versailles, France (T.V., E.F.C., H.T., E.B., T.D., H.H., M.G., S.V.); and Wageningen University and Research Plant Breeding, Wageningen University and Research Centre, 6708 PD Wageningen, The Netherlands (N.M., L.M.T.)

Plant growth and organ formation depend on the oriented deposition of load-bearing cellulose microfibrils in the cell wall. Cellulose is synthesized by a large relative molecular weight cellulose synthase complex (CSC), which comprises at least three distinct cellulose synthases. Cellulose synthesis in plants or bacteria also requires the activity of an endo-1,4- β -D-glucanase, the exact function of which in the synthesis process is not known. Here, we show, to our knowledge for the first time, that a leaky mutation in the Arabidopsis (*Arabidopsis thaliana*) membrane-bound endo-1,4- β -D-glucanase KORRIGAN1 (KOR1) not only caused reduced CSC movement in the plasma membrane but also a reduced cellulose synthesis inhibitor-induced accumulation of CSCs in intracellular compartments. This suggests a role for KOR1 both in the synthesis of cellulose microfibrils and in the intracellular trafficking of CSCs. Next, we used a multidisciplinary approach, including live cell imaging, gel filtration chromatography analysis, split ubiquitin assays in yeast (*Saccharomyces cerevisiae* NMY51), and bimolecular fluorescence complementation, to show that, in contrast to previous observations, KOR1 is an integral part of the primary cell wall CSC in the plasma membrane.

Cellulose microfibrils are synthesized by a hexameric multiprotein complex at the plasma membrane called the cellulose synthase complex (CSC). Genetic analysis, expression data, and coimmunoprecipitation experiments have demonstrated that a functional CSC contains at least three different nonredundant cellulose synthase (CESA) isoforms (H ofte et al., 2007). CESA1, CESA3, and CESA6-like are involved in cellulose biosynthesis during primary cell wall deposition, whereas CESA4, CESA7, and CESA8

are essential for cellulose synthesis in the secondary cell wall (Taylor et al., 1999, 2000, 2003; Desprez et al., 2007; Persson et al., 2007). CSCs labeled by fluorescently tagged CESA proteins migrate in the plasma membrane along cortical microtubules (CMTs), propelled by the polymerization of the β -1,4-glucans (Paredez et al., 2006). Partial depolymerization of CMTs using oryzalin showed that the organized trajectories of CSCs depend on the presence of an intact CMT array. The CSC-microtubule interaction is mediated at least in part by a large protein, POMPOM2/CELLULOSE SYNTHASE INTERACTING1, that binds to both CESAs and microtubules (Lei et al., 2014). Interestingly, complete depolymerization of CMTs does not alter the velocity of the complexes, illustrating that CMTs are necessary for the guidance of CSCs but not for their movement (Paredez et al., 2006). The microtubule cytoskeleton also has a role in the secretion and internalization of CSCs (Crowell et al., 2009; Gutierrez et al., 2009)

KORRIGAN1 (KOR1) is a membrane-bound endo-1,4- β -D-glucanase (EGase) that is also required for cellulose synthesis (Nicol et al., 1998). Enzymatic analysis of a recombinant and soluble form of the *Brassica napus* KOR1 homolog showed substrate specificity for low-substituted carboxymethyl cellulose and amorphous cellulose but no activity on crystalline cellulose, xyloglucans, or short cellulose oligomers (M olh oj et al., 2001; Master et al., 2004). Fractionation of microsomes demonstrated that KOR1 is primarily present in plasma membrane fractions but also at low levels in a tonoplast-enriched fraction (Nicol et al.,

¹ This work was supported by IMACEL (grant no. ANR-06-BLAN-0262).

² These authors contributed equally to the article.

³ Present address: Swedish University of Agricultural Sciences, Department of Forest Genetics and Plant Physiology, Ume  Plant Science Center, 901 83 Umea, Sweden.

⁴ Present address: Institut de G en tique et Microbiologie, Unit e Mixte de Recherche 8621-Centre National de la Recherche Scientifique Universit  Paris-Sud 11, 91400 Orsay, France.

⁵ Present address: Energy Biosciences Institute, University of California, Berkeley, CA 94720.

⁶ Present address: Department of Biology, Columbia University, New York, NY 10027.

* Address correspondence to samantha.vernhettes@versailles.inra.fr.

The author responsible for distribution of materials integral to the findings presented in this article in accordance with the policy described in the Instructions for Authors (www.plantphysiol.org) is: Samantha Vernhettes (samantha.vernhettes@versailles.inra.fr).

[W] The online version of this article contains Web-only data.

www.plantphysiol.org/cgi/doi/10.1104/pp.114.241216

1998). Similarly, the KOR1 ortholog from tomato (*Solanum lycopersicum*) was found in the plasma membrane and fractions enriched for the Golgi apparatus (Brummell et al., 1997). A GFP-KOR1 fusion protein expressed with the Cauliflower mosaic virus 35S promoter accumulated in the Golgi apparatus and post-Golgi compartments and the tonoplast (Robert et al., 2005). Surprisingly for an enzyme involved in cellulose synthesis, the protein could not be detected at the plasma membrane. Using this construct, it was also shown that KOR1 undergoes regulated intracellular cycling (Robert et al., 2005).

Although numerous genetic studies indicate that KOR1 is required for cellulose synthesis in primary and secondary cell walls and during cell plate formation (Nicol et al., 1998; Peng et al., 2000; Zuo et al., 2000; Lane et al., 2001; Sato et al., 2001; Szyjanowicz et al., 2004), its precise role in the cellulose synthesis process remains unclear. It has been suggested that KOR1 might be a component of the CSC (Read and Bacic, 2002). However, until now there has been no experimental evidence for this in *Arabidopsis thaliana*, either with co-precipitation experiments or with localization studies (Szyjanowicz et al., 2004; Robert et al., 2005; Desprez et al., 2007). Numerous hypotheses have been proposed to explain the paradoxical role of KOR1 in cellulose synthesis (Robert et al., 2004). KOR1 might have a proofreading activity involved in hydrolyzing disordered amorphous cellulose to relieve stress generated during the assembly of glucan chains in cellulose microfibrils (Mølhøj et al., 2002). Alternatively, KOR1 may determine the length of individual cellulose chains, either during cellulose synthesis or once the microfibril has been incorporated in the wall. A third hypothesis is that KOR1 releases the cellulose microfibril from the CSC before the complex is internalized from the plasma membrane (Somerville, 2006). Studies in cotton (*Gossypium hirsutum*) fiber extracts identified sitosterol glucoside as a primer for the cellulose synthesis and suggested that KOR1 could be involved in their cleavage from the nascent glucan chain (Peng et al., 2002). However, this scenario is unlikely, since, at least for the bacterial CESA, which is homologous to plant CESAs, there is no evidence for the existence of lipid-linked precursors, as shown by the three-dimensional structure of an active complex (Morgan et al., 2013).

In this study, we first confirmed previous observations (Paredes et al., 2008) that, in the leaky *kor1-1* mutant, the velocity of the CSCs is reduced compared with that in a wild-type background but that, in addition, the mutation affects the ability of the cellulose synthesis inhibitor CGA325'615 (hereafter referred to as CGA) to induce the accumulation of GFP-CESA3 in a microtubule-associated compartment (MASC/small compartments carrying cellulose synthase complexes [SmaCCs]; Crowell et al., 2009; Gutierrez et al., 2009). This indicates that KOR1 plays a role both in the synthesis of cellulose and in the intracellular trafficking of the CSC. Using gel filtration approaches, we identified KOR1 in fractions of high molecular mass, suggesting that KOR1 is present in membranes as part

of a protein complex. We next analyzed the dynamics of GFP-KOR1 expressed in the *kor1-1* mutant background under the control of its endogenous promoter. GFP-KOR1 is found in discrete particles at the plasma membrane in the same cells as GFP-CESAs (Crowell et al., 2009). GFP-KOR1 plasma membrane particles migrate along linear trajectories with comparable velocities to those observed for GFP-CESAs. The organization of GFP-KOR1 at the plasma membrane also requires the presence of an intact microtubule array, suggesting that KOR1 and CESA trajectories in the plasma membrane are regulated in the same manner. GFP-KOR1 and mCherry-CESA1 partially colocalize in the plasma membrane, Golgi, and post-Golgi compartments. Finally, we provide evidence for direct interaction between KOR1 and primary cell wall CESA proteins using the membrane-based yeast (*Saccharomyces cerevisiae* NMY51) two-hybrid (MbYTH) system (Timmers et al., 2009) and bimolecular fluorescence complementation (BiFC). Our data support a new model in which KOR1 is an integral part of the CSC, where it plays a role not only in the synthesis of cellulose but also in the intracellular trafficking of the CSC.

RESULTS

KOR1 Is Required for Normal CSC Activity and CGA-Induced Accumulation in Intracellular Compartments

Leaky mutants in *KOR1* show reduced growth and reduced cellulose content (Nicol et al., 1998; Lane et al., 2001; Sato et al., 2001), but the exact function of the KOR1 protein in cellulose biosynthesis remains unclear. We expressed a GFP-CESA3 fusion protein in wild-type and *kor1-1* backgrounds to study the movement of the CSCs in the plasma membrane as a read-out of their activity in real time. In the wild-type background, GFP-CESA3 was present in the plasma membrane in fluorescent punctae, which showed a bidirectional movement at a constant average rate of 253 nm min^{-1} ($n = 540$; Fig. 1, A, C, and E). In the *kor1-1* background, a comparable coverage of GFP-CESA3 punctae was detected (Fig. 1, A and F), but their velocity was significantly reduced (Fig. 1, C and E), with an average of around 147 nm min^{-1} ($n = 514$), indicating that KOR1 is required for the normal motility of the CSCs. We next investigated whether KOR1 has a role in the intracellular trafficking of CSCs. To this end, we treated seedlings with the cellulose synthesis inhibitor CGA, which is known to promote the removal of the CSCs from the plasma membrane and their accumulation in the MASCs (Crowell et al., 2009). As shown previously, a 5-h treatment with 5 nM CGA had cleared all of the GFP-CESA3 signal from the plasma membrane in favor of its accumulation in MASCs/SmaCCs, which could be identified in kymographs based upon their characteristic linear and erratic movement (Fig. 1, B and D). In *kor1-1*, GFP-CESA3 had also disappeared from the plasma membrane to accumulate in intracellular compartments, some of which were

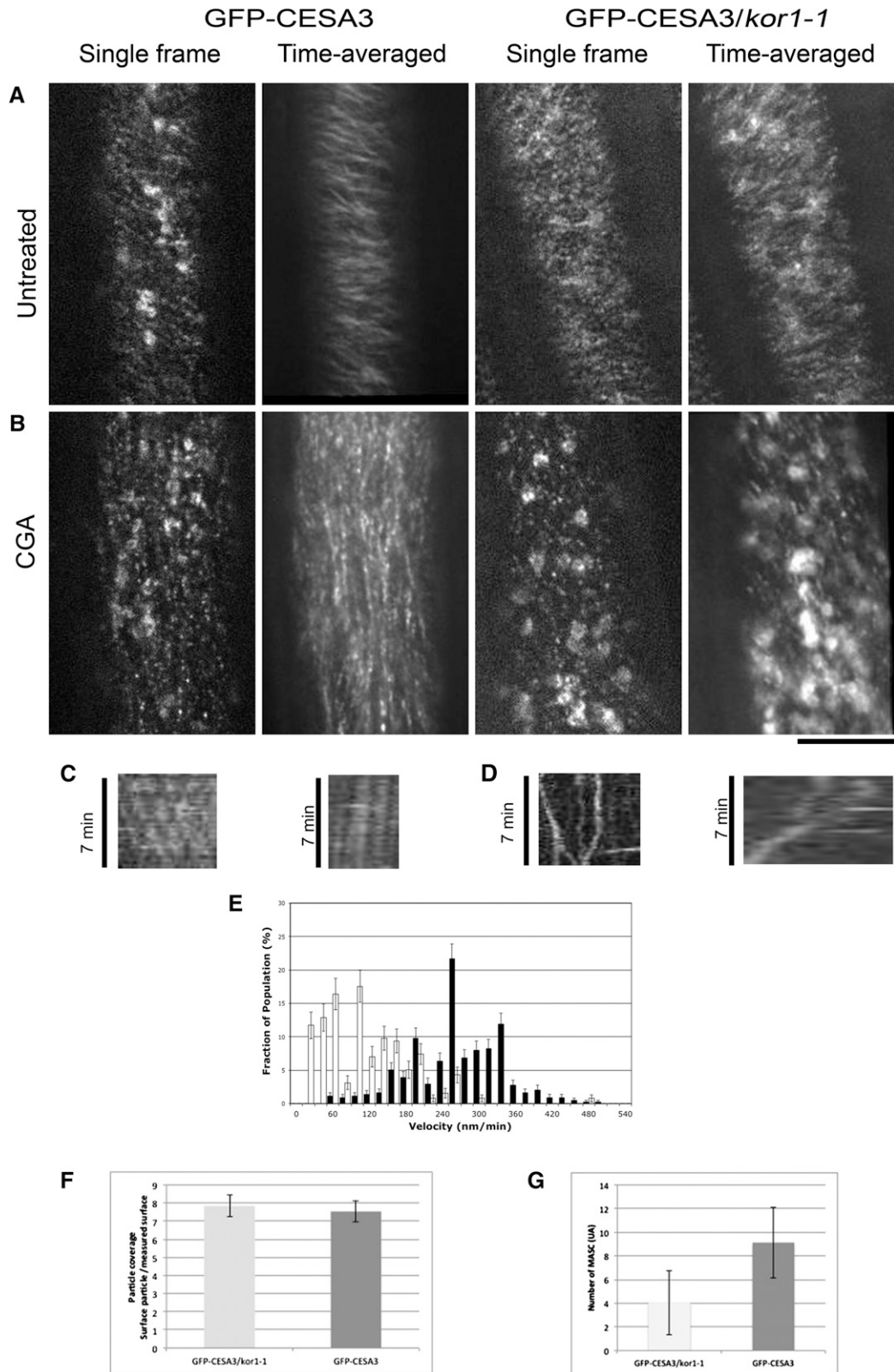


Figure 1. KOR1 is required for normal CSC motility and CGA-induced accumulation in intracellular compartments. A and B, Single optical sections and average projections of time series (61 frames) of GFP-CESA3 in wild-type and *kor1-1* controls (A) and after 5 h of CGA treatment (B). Bar = 10 μ m. C and D, Kymographs along GFP-CESA3 trajectories in wild-type (left) and *kor1-1* (right) controls (C) and after 5 h of CGA treatment (D). E, Histogram of GFP-CESA3 particle velocities. The mean velocity is

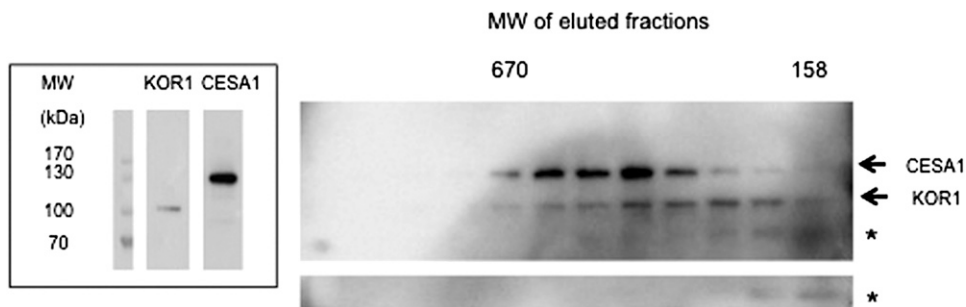


Figure 2. KOR1 and CESA1 are present in a high molecular mass protein complex in Arabidopsis seedlings. A, KOR1 and CESA1 are detectable as approximately 100- and 120-kD bands, respectively, in denatured total membrane protein extracts from Arabidopsis seedlings revealed by α NKOR and α CESA1 antibodies. B, Gel filtration profiles of KOR1 in 4-d-old Arabidopsis seedlings. Solubilized microsomes were fractionated on a Superdex 200 30/300 GL column. Eluted fractions were analyzed by immunoblotting with α NKOR and α CESA1 antibodies. The Superdex 200 column was calibrated with gel filtration standards (indicated at the top). Both KOR1 and CESA1 are present in high molecular mass protein complexes. Note the presence of KOR1 degradation products (asterisks) recognized by α NKOR.

identified as MASCs/SmaCCs (Fig. 1, B and D). However, an over 2-fold reduction in the number of GFP-CESA3-labeled MASCs was observed in the mutant as compared with the wild-type background, indicating that KOR1 is not only involved in the synthesis of cellulose but also required for the intracellular relocalization of the CSC upon CGA treatment (Fig. 1G).

KOR1 Is Present in a High Molecular Mass Complex in Arabidopsis and Cotton

Since previous coimmunoprecipitation attempts to detect an interaction between CSC and KOR1 had failed (Desprez et al., 2007), we first used a gel filtration approach to investigate whether KOR1 is part of a protein complex. Crude microsomal membranes were extracted from 4-d-old dark-grown seedlings, solubilized with 0.5% Triton X-100, and loaded on a gel filtration column. Immunoblot analysis of the eluted fractions with an antibody raised against the N-terminal cytoplasmic domain of KOR (α NKOR) showed that KOR1 was present in high-molecular mass fractions from 70 to 670 kD, with a maximum in the fractions corresponding to approximately 158 kD (Fig. 2). This estimated molecular mass was higher than the one expected for the KOR1 monomeric protein, suggesting that KOR1 is part of a membrane protein complex. Using α CESA1 antibody, we detected a signal that overlapped with the α NKOR signal in higher molecular

mass fractions, with a maximum in the fractions corresponding approximately to 400 kD. Interestingly, α NKOR also recognized smaller fragments corresponding to degradation products (Fig. 2, asterisks), but only in the lower molecular mass fractions containing KOR1, suggesting that KOR1 in the lower molecular mass fractions was more susceptible to proteolysis than in intact complexes. These results, therefore, do not exclude that a fraction of KOR1 is present in the same complex as CESA1. To corroborate these observations in a different system, we focused on cotton fibers, which produce large amounts of cellulose (mature cell walls consist of 95% cellulose) in a developmentally controlled way. The α NKOR antibody detected a protein of the expected size during all the distinct growth stages 5, 10, 15, 20, 25, and 30 DPA (Supplemental Fig. S1A). A dramatic increase in the signal was observed between 15 and 20 DPA, corresponding to the transition period between cell elongation and massive cellulose synthesis during secondary cell wall deposition. Size-exclusion chromatography fractionation also revealed the presence of a cross-reacting protein in a high molecular mass complex of around 400 kD in elongating fibers (10, 15, and 20 DPA) but also at 25 DPA, when cellulose deposition peaks (Supplemental Fig. S1B). Remarkably, at the time point at which the fiber has reached a terminal developmental stage (30 DPA) and during which the rate of cellulose drops sharply (Meinert and Delmer, 1977), the α NKOR ligand was present in a smaller molecular mass fraction of around 160 kD.

Figure 1. (Continued.)

253 nm min⁻¹ in the wild type ($n = 540$; black bars) and 147 nm min⁻¹ in *kor1-1* ($n = 514$; white bars). Note that the two values are significantly different (Student's t test, $P = 2.2 \times 10^{-16}$). F, Coverage of GFP-CESA3 particles in the wild type ($n = 42$) and *kor1-1* ($n = 45$). Note that the two densities are not significantly different (Student's t test, $P = 0.93$). G, Histogram of the number of MASCs (defined as intracellular particles with erratic movement) expressed in arbitrary units (UA). The number of GFP-CESA3-containing MASCs upon CGA treatment is significantly lower in the *kor1-1* background ($n = 254$) compared with the wild-type background ($n = 245$; Student's t test, $P = 210^{-16}$).

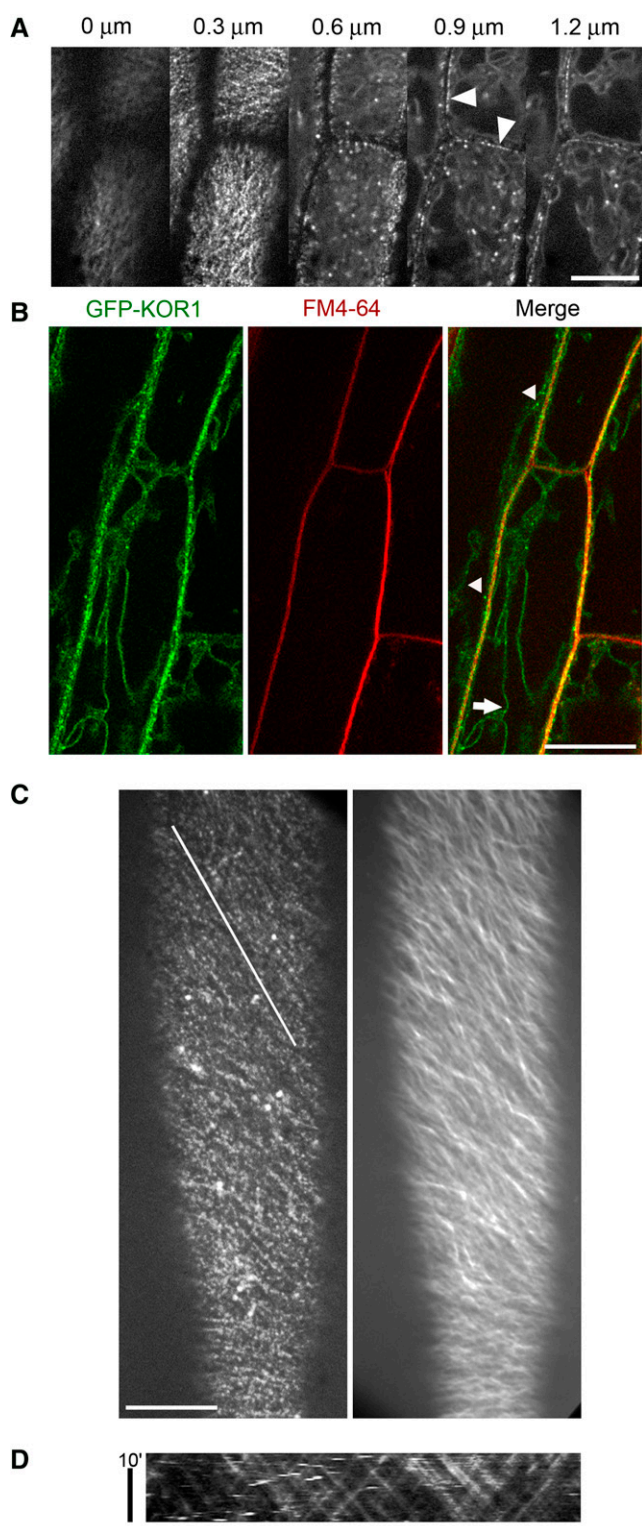


Figure 3. KOR1 migrates within the plasma membrane. Images were acquired in the hypocotyl epidermis of 3-d-old etiolated *Arabidopsis* seedlings expressing GFP-KOR1 in the *kor1-1* mutant background. A, Successive optical sections (0.3- μm interval) of a z-stack through epidermal cells at the top of the hypocotyl. GFP-KOR1 particles are dense in the plasma membrane. In deeper optical sections, the plasma membrane labeling of GFP-KOR1 is also visualized at the periphery of

Together, these data indicate that KOR1 was at least partially present in a high molecular mass complex both in *Arabidopsis* seedlings and in cotton fibers. In *Arabidopsis*, both KOR1 and CESA1 were present in the same higher molecular mass fractions. In cotton, the size of the complex was comparable during primary and secondary cell wall synthesis, and KOR1 dissociated from at least part of the complex at the end of fiber development.

KOR1 Is Present in the Plasma Membrane and Intracellular Compartments

To gain insight into the possible role of KOR1 in cellulose synthesis, we first sought to determine where it is localized in cells and where it might exert its activity. We expressed a GFP fusion (GFP-KOR1) under the control of its endogenous promoter in the *kor1-1* mutant background. The construct partially complemented the dark-grown hypocotyl phenotype of *kor1-1*, indicating that the fusion protein was at least partially functional (Supplemental Fig. S2; for a discussion of the potential implications of the lack of complete complementation, see below). Examination of GFP-KOR1 in the epidermis of 3-d-old etiolated hypocotyls revealed, in contrast to previous observations of an overexpressed GFP-KOR1 construct expressed from the Cauliflower mosaic virus 35S promoter, the presence of discrete particles aligned at the surface of the cells, in the focal plane of the plasma membrane (Fig. 3A). We confirmed the plasma membrane localization of these particles by showing colocalization with the lipophilic tracer dye FM4-64 (Bolte et al., 2004; Fig. 3B). In addition, GFP-KOR1 also accumulated in intracellular particles (Fig. 3B, arrowheads; Supplemental Fig. S3) and the tonoplast (Fig. 3B, arrow). To identify those compartments, we crossed the GFP-KOR1-expressing lines into a set of mCherry/monomeric red fluorescent protein-tagged marker lines. The results show that GFP-KOR1 colocalized with the Golgi marker glutamic-oxaloacetic transaminase1 homolog (Geldner et al., 2009; Supplemental Fig. S3A), the early endosome/trans-Golgi network marker vacuolar H-ATP synthase isoform a1 (Dettmer et al., 2006; Supplemental Fig

the cells (arrowheads). B, Cells at the top of the hypocotyl labeled with FM4-64. In the merged images, GFP-KOR1 clearly colocalizes with FM4-64 at the plasma membrane. GFP-KOR1 also accumulated in intracellular compartments (arrowheads) and the tonoplast (arrow). C, The left image shows a single time point from a time series. GFP-KOR1 particles are aligned in rows in the plasma membrane. In the right image, an average projection of the time series illustrates the movement of GFP-KOR1 particles with linear trajectories. D, Kymograph along the trajectory indicated by the white line in C. Position is represented along the z axis, and time is represented along the y axis. The cross-hatched pattern indicates that GFP-KOR1 particles move bidirectionally with steady velocities. Bars = 10 μm .

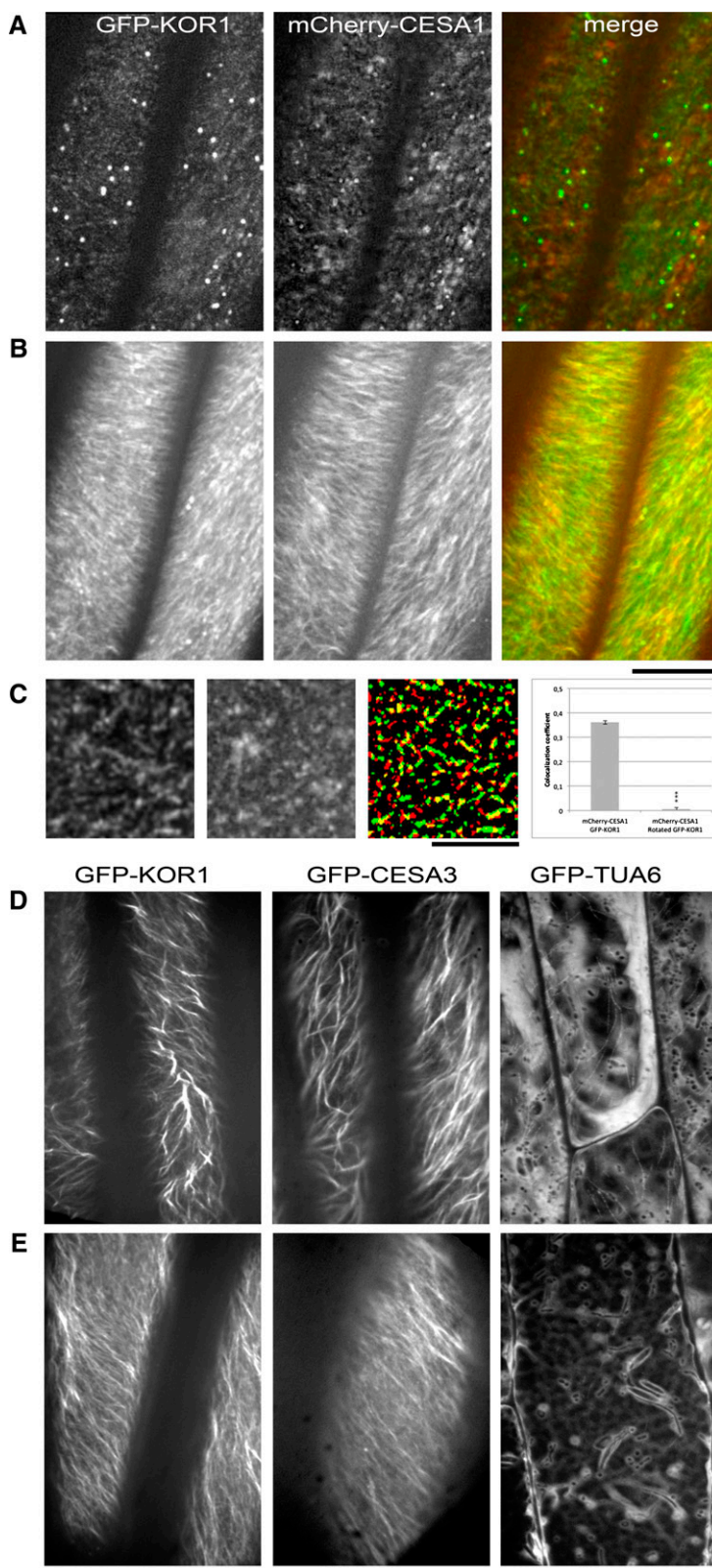


Figure 4. GFP-KOR1 plasma membrane trajectories overlap with the trajectories of mCherry-CESA1. Images were acquired at the surface of hypocotyl epidermis in 3-d-old etiolated *Arabidopsis* seedlings. A and B, Single optical sections acquired (A) and average projections of time series (B) in plants expressing both GFP-KOR1 (left) and mCherry-CESA1 (middle). The merged images are shown at right. C, Denoised single optical sections: GFP-KOR1 (left), mCherry-CESA1 (middle), and merged (right).

S3B), and the prevacuolar compartment (PVC) marker Rab-GTP synthase G3c (Geldner et al., 2009; Supplemental Fig. S3D). Interestingly, GFP-KOR1 weakly colocalized with the early endosome marker RabA1g (Geldner et al., 2009; Supplemental Fig. S3C). Upon treatment with the cellulose synthesis inhibitor CGA, a majority of the GFP-KOR1-labeled particles colocalized with microtubules (Supplemental Fig. S3E) and showed the erratic movement of the MASCs/SmaCCs (Supplemental Fig. S3F). Together, these results demonstrate the complex regulation of the intracellular trafficking of GFP-KOR1. Indeed, it migrates between Golgi stacks, post-Golgi compartments, MASCs/SmaCCs, and the plasma membrane. In addition, GFP-KOR1 is deviated into the degradation pathway represented by the PVC and the tonoplast.

GFP-KOR1 Plasma Membrane Particles Have the Same Velocity as GFP-Tagged CESA Complexes

Visualization of time series showed that GFP-KOR1 plasma membrane particles are motile (Fig. 3C; Supplemental Movie S1). We analyzed their movement in the hypocotyl epidermis of 3-d-old etiolated seedlings using kymographs. The straight traces on the kymographs and the cross-hatched pattern indicate that GFP-KOR1 plasma membrane particles migrated bidirectionally along linear tracks with steady velocities (Fig. 3D). Five hundred forty-five measurements from 12 cells in four plants gave a mean velocity of 280 nm min^{-1} for GFP-KOR1 plasma membrane particles (range, $111\text{--}439 \text{ nm min}^{-1}$). Notably, the mean velocity and velocity range are similar to those observed for GFP-CESA3 and GFP-CESA6, two CESAs involved in the deposition of the primary cell wall (277 and 272 nm min^{-1} , respectively; Desprez et al., 2007). Likewise, the trajectories of GFP-KOR1 plasma membrane particles, like those of GFP-CESA3 in the same cell types, overlapped mostly with cortical microtubules (Supplemental Fig. S4, A–C). GFP-KOR1 and GFP-CESA3 trajectories both showed a range of orientations in elongating cells (Supplemental Fig. S4A) and adopted strictly longitudinal orientations in cells at the base of the hypocotyl (Supplemental Fig. S4, B and C). Taken together, these results indicate that GFP-KOR1 follows the microtubule reorientation

during epidermal cell elongation, as shown previously with the CSCs labeled by GFP-CESA3.

KOR1 Is Associated with CESA Complexes

Thus far, the presence of KOR1 in a high molecular mass complex and the localization and motility of GFP-labeled KOR1 plasma membrane particles favor the hypothesis that KOR1 associates with primary CSC. To investigate this in more detail, we expressed a chimeric mCherry-CESA1 protein under the control of its endogenous promoter in the *cesa1^{rswt-10}* mutant background. The construct complemented the dark-grown hypocotyl phenotype of the mutant, indicating its functionality (Supplemental Fig. S5). We then examined the localization of both GFP-KOR1 and mCherry-CESA1 in double transformants. In epidermal cells, GFP-KOR1 plasma membrane trajectories overlapped substantially with those of mCherry-CESA1 (Fig. 4, A and B; Supplemental Movie S2). The calculation of a colocalization coefficient on a small bright circular signal showed a partial colocalization between GFP-KOR1 punctae and those of mCherry-CESA1 in the plasma membrane (Fig. 4C) and no colocalization when the image was rotated 90° , suggesting that the partial colocalization does not result from random overlap. One trivial explanation for the overlapping trajectories of GFP-KOR1 and mCherry-CESA1 plasma membrane particles could be that both proteins are guided by cortical microtubules as they move independently through the plasma membrane. Since EGase activity is not predicted as such to confer motility to GFP-KOR1 plasma membrane particles, we asked if GFP-KOR1 movement might depend on microtubule motor proteins. To test this possibility, we depolymerized cortical microtubules using $7 \mu\text{M}$ oryzalin and studied the movement of GFP-KOR1 plasma membrane particles. The mean velocity of GFP-KOR1 did not change significantly (mean = 262 nm min^{-1} ; $n = 709$), indicating that the GFP-KOR1 movement occurred independently from microtubule motors. However, GFP-KOR1-expressing seedlings and GFP-CESA3-expressing seedlings exposed to the same oryzalin treatments exhibited a similar disorganization of the trajectories of plasma membrane particles (Fig. 4, D and E). At early time points in the treatment, both GFP-CESA3 and GFP-KOR1 accumulated along specific high-density tracks (Fig. 4D). At later time points, both

Figure 4. (Continued.)

The graph presents the average Pearson's coefficient with se ($n = 7$). The superposition of the two binary images shows partial overlap between the extracted signals and no colocalization when the GFP-KOR1 image is rotated 90° (Student's t test, $P = 5 \times 10^{-13}$). Bar = $2.5 \mu\text{m}$. D and E, The left images show average projections of time series acquired in plants expressing GFP-KOR1, the middle images present average projections of time series acquired in plants expressing GFP-CESA3, and the right images show maximum projected z-stacks of GFP-TUA6-labeled microtubules in the same cell types. D, Treatment with $7 \mu\text{M}$ oryzalin for 6 h leads to partial depolymerization of cortical microtubules (right) and disorganization of the trajectories of GFP-KOR1 plasma membrane particles (left) and GFP-CESA3 plasma membrane particles (middle) in a similar manner. E, Treatment with $7 \mu\text{M}$ oryzalin for 10 h completely depolymerizes the cortical microtubule array (right). In these conditions, GFP-KOR1 (left) and GFP-CESA3 (middle) plasma membrane particles have a more parallel orientation than after the 6-h treatment. Bars = $10 \mu\text{m}$ except where noted.

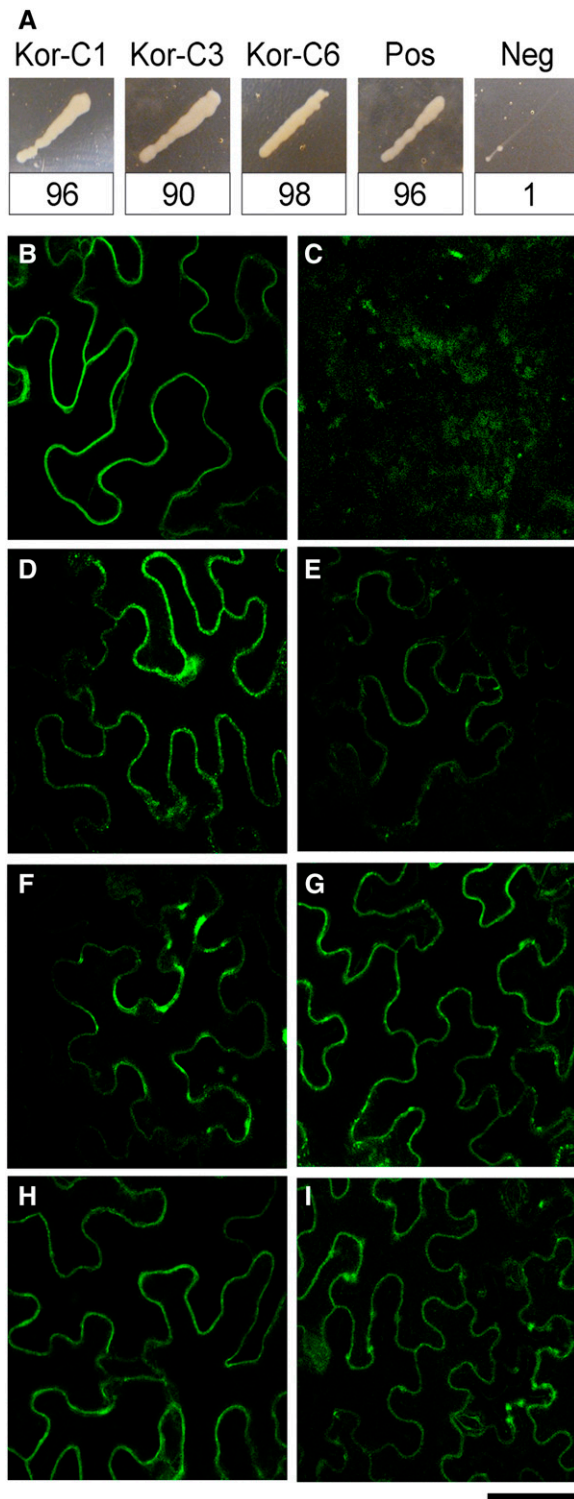


Figure 5. KOR1 interacts with CESA proteins in yeast and in planta. A, KOR1 interacts with primary CESA proteins in yeast. A split-ubiquitin assay for interactions between membrane-bound proteins is shown. The numbers of colonies capable of growing on nutrient-deficient medium were counted in strains expressing KOR1 and CESA proteins fused to the N or C terminus of ubiquitin (see “Materials and Methods”). Yeast is able to grow only when the two expressed proteins interact (e.g. in the positive control [POS]). Neg, Negative control. B to I,

fluorescent proteins showed more organized trajectories, as observed previously (Paredes et al., 2006; Fig. 4E). Therefore, as for the CSCs, the motility of GFP-KOR1 plasma membrane particles was independent of cortical microtubule motors and, hence, also depended on the activity of the CSC complex, which suggests a close physical interaction.

To verify that KOR1 and CESA1, CESA3, or CESA6 can interact, we first used the split-ubiquitin method to test if CESA and KOR1 were capable of interacting *in vivo* in yeast. KOR1 was fused to the C-terminal fragment of ubiquitin alongside a transcription factor (the bait). CESA1, CESA3, and CESA6 proteins were each fused to the N-terminal part of ubiquitin (the prey). If the bait and prey proteins interact, the transcription factor will be cleaved from the bait protein and activate the expression of genes that allow the yeast strain to grow on selective medium. As a negative control, we tested KOR1 as bait and an unrelated protein, Asparagine-linked glycosylation5, as prey (Timmers et al., 2009). The yeast strains failed to grow in multiple repetitions of this experiment, demonstrating that a specific interaction between the bait and prey is required to activate the system (Fig. 5A). In contrast, when CESA1, CESA3, or CESA6 was used as prey, the yeast strains were able to grow on the selective medium, indicating that KOR1 interacts specifically with each of these three CESA isoforms (Fig. 5A). Reverse experiments, in which the CESA protein was expressed as bait and KOR1 as prey, also permitted growth of the yeast strains. We conclude that KOR1 can interact with CESA1, CESA3, and CESA6 in yeast.

To verify that KOR1 and CESA1, CESA3, or CESA6 can interact in planta, we used BiFC (Desprez et al., 2007). Using this technique, fluorescence is revealed only if two proteins fused to split yellow fluorescent protein (YFP) interact. Positive and negative controls testing the dimerization of plasma membrane intrinsic proteins2-1 (PIP2-1) protein (Fig. 5B) and the interaction of PIP2-1 with CESA1 (Fig. 5C), respectively, both yielded the expected result. YFP fluorescence was consistently obtained when KOR1 and CESA1 interactions were tested, regardless of the vector combination (Fig. 5, D and E). The fluorescent signal was localized to the plasma membrane and to punctate structures in the cytoplasm. Since KOR1

KOR1 interacts with CESA proteins in planta. B and C, BiFC experiments in tobacco leaf epidermis are shown. Confocal images are presented, showing YFP fluorescence indicating an interaction (e.g. in the positive control testing the dimerization of PIP2 (B)) or the lack of fluorescence indicating no interaction (e.g. in the negative control testing the interaction between PIP2 and CESA1 [C]). D and E, Test for interaction between KOR1 and CESA1 by fusing KOR1 to the N terminus of YFP and CESA1 to the C terminus of YFP (D) or the reverse (E). F and G, Test for interaction between KOR1 and CESA3 by fusing KOR1 to the N terminus of YFP and CESA3 to the C terminus of YFP (F) or the reverse (G). H and I, Test for interaction between KOR1 and CESA6 by fusing KOR1 to the N terminus of YFP and CESA6 to the C terminus of YFP (H) or the reverse (I). Bar = 37 μ m.

Table 1. Primers used for the MbYTH system

Genes	Primers
	Primers for KOR1 amplification (BiFC)
<i>KOR1</i>	5'-AAAAAAGCAGGCTCCATGTACGGAAAGAGATCCATGGGGAGGT-3' 5'-AAGAAAGCTGGGTGCTGTTCCATGGTGCTGGTGGAGGGGTGGTGG-3'
	Primers for bait amplification
<i>CESA1</i>	5'-AAGACTGCAGAATGGAGGCCAGTGCCGGC-3' 5'-AACAGGCGCCCTAAAAGACACCTCCTTTGCC-3'
<i>CESA3</i>	5'-AGAACCATGGAATGGAATCCGAGGAGAAACC-3' 5'-AAGAAGTGTCAACAGTTGATTCCACTCC-3'
<i>CESA6</i>	5'-AGAACCATGGAATGAACACCGGTGGTCCGG-3' 5'-AAGAAGTGTCAACAAGCAGTCTAAACCA-3'
<i>KOR1</i>	5'-AAGACGTCATGTACGGAAGAGATCCATGGGG-3' 5'-TTTACTAGTCAAGTTTCCATGGTGCTGGTGG-3'
	Primers for prey amplification
<i>CESA1</i>	5'-AAGAGGCCATTACGGCCATGGAGGCCAGTGCCGGC-3' 5'-AAGAGGCCGAGGCGGCCAAGTAAAAGACACCTCCTTTGCCAT-3'
<i>CESA3</i>	5'-AGAACGGCCATTACGGCCATGGAATCCGAAGGAGAAACC-3' 5'-GAGGCCGAGGCGGCCGTCAACAGTTGATTCCACATTCCAGAAT-3'
<i>CESA6</i>	5'-AGAACGGCCATTACGGCCATGAACACCGGTGGTCCGGTTAATCGC-3' 5'-GAGGCCGAGGCGGCCGTCAACAAGCAGTCTAAACCACAGATCTCGAGAAT-3'
<i>KOR1</i>	5'-AACAGGCCATTACGGCCATGTACGGAAGAGATCCATGGGG-3' 5'-AAGAGGCCGAGGCGGCCATCAAGTTTCCATGGTGCTGGTGG-3'

and CESA proteins normally traffic to the plasma membrane, the presence of signal at this subcellular location is a positive indication that the proteins were correctly folded and transported. In contrast to CESA1, interaction with CESA3 or CESA6 was less reproducible: positive signals were observed in only five out of 10 experiments (Fig. 5, F–I). We conclude that KOR1 indeed can interact physically in planta with the primary cell wall CSC and that this might preferentially occur through an interaction with CESA1.

DISCUSSION

In this study, the following evidence shows that KOR1 is an integral part of the CSC: gel filtration of cotton fiber extracts showed that KOR1 was present in high molecular mass complexes and in extracts from Arabidopsis seedlings, and high molecular mass fractions contained both KOR1 and CESA1; GFP-KOR1 was present in punctae in the plasma membrane that migrated along microtubules at the same velocity as GFP-CESA1-containing punctae, both of which moved independently from microtubule motors; GFP-KOR1 also colocalized in part with mCherry-CESA1, and yeast split-ubiquitin assays and in planta BiFC showed a direct interaction between KOR1 and CESAs. In contrast, coimmunoprecipitation experiments so far have revealed interactions only between the three distinct CESA proteins (Taylor et al., 2003; Desprez et al., 2007) and failed to show interactions with other CSC components such as cellulose synthase interactive1 or KOR1. This suggests that the interactions between KOR1 and CESAs are more labile than those among CESAs themselves or may require the presence of other components such as certain membrane lipids, as observed for tetraspannin membrane complexes in animal cells, the

stability of which depends on the presence of cholesterol (Charrin et al., 2003). It should be noted that GFP-KOR1 expressed from its endogenous promoter was not completely functional, as shown by the only partial complementation of the dark-grown hypocotyl phenotype of *kor1-1*. This may imply that the GFP tag affects the trafficking and/or dynamics of KOR1 and, hence, that the results should be interpreted with caution. Nevertheless, the main message of this study, the association of KOR1 with the CSC, is corroborated by several lines of evidence.

The association of KOR1 with CSCs at the plasma membrane suggests that KOR1 is intimately involved in the synthesis of glucan chains and/or their assembly into microfibrils. Such a role is indeed corroborated by the reduced velocity of GFP-CESA3 in a *kor1-1* mutant background compared with the wild type, considering that this velocity is a measure for activity if we assume that the energy for the CSC movement is provided by the polymerization of the glucan chains and the crystallization of the microfibrils (Diotallevi, 2007). In this context, the role for an EGase could be the untangling of aberrantly associated glucan chains upon emergence from the 18 or more CESA subunits that constitute a CSC (Newman et al., 2013). Modeling showed that the formation of an amorphous intermediate through the random interaction of emerging glucan chains on top of the CSC is compatible with the assembly of an ordered microfibril later on (Haigler et al., 2014). In such a scenario, EGase activity on noncrystalline glucans might prevent the interaction among glucan chains from adjacent CSCs within the plasma membrane and, hence, the aberrant association of multiple microfibrils, which also could lead to the slowing down of the deposition rate. In a similar way, an EGase has been implicated in microfibril assembly in the cellulose-producing bacterium *Gluconacetobacter xylinus* (Nakai et al., 2013). Another interesting observation is the

reduced accumulation of GFP-CESA3 in MASCs upon treatment with the cellulose synthesis inhibitor CGA. This accumulation reflects the inhibition of secretion and/or accelerated internalization of CSCs (Crowell et al., 2009; Gutierrez et al., 2009). In this context, it should be noted that recent observations of the three-dimensional structure of a bacterial CESA complex (the catalytic subunit of which is homologous to plant CESAs) show that 18 residues of each nascent glucan chain are embedded inside a translocation channel within the CESA complex (Morgan et al., 2013). Considering that this would be true for the 18 or more glucan chains produced by the CSC, the interaction between CSC and cellulose microfibril must be extremely strong. Therefore, it is difficult to imagine how during internalization the CSC could detach from the cell wall-bound cellulose microfibril in the absence of an enzymatic cleavage of the glucan chains. The reduced ability of GFP-CESA3 to accumulate in MASCs in the leaky mutant *kor1-1* could reflect at least in part the impaired ability of CSCs to detach from the cell wall during this process.

We observed the accumulation of GFP-KOR1 in plasma membrane-associated punctae and in various intracellular compartments, including Golgi bodies and the post-Golgi compartments trans-Golgi network and MASCs, which may play a role in the recycling of CSCs. The weak colocalization with the early endosome marker RabA1g suggests that KOR1, and presumably the CSCs, transit rapidly through this compartment upon internalization or use an alternative route. Finally, and in contrast to GFP-CESA, GFP-KOR1 was found also in compartments involved in protein turnover: the PVC and vacuole. Together, these observations are consistent with our previous findings on GFP-KOR1 expressed from the *35S* promoter, with the difference that we failed to observe an accumulation of the fluorescent signal in the plasma membrane. This failure might be related to the deregulation of the intracellular trafficking of KOR1 due to the higher expression level of the *35S::GFP-KOR1* construct. Interestingly, the intracellular distribution of GFP-KOR1 only partially overlapped with that of GFP-CESA, as shown by the presence of GFP-KOR1 in the PVC and tonoplast, in which GFP-CESA did not accumulate. This suggests the dissociation of KOR1 from other CSC components along the secretory pathway. Such a transient interaction was also suggested by the release of KOR1 from high molecular mass complexes at the final stages of cotton fiber maturation and the presence of a KOR1 degradation product only in the low molecular mass fractions from size-exclusion chromatography. It will be interesting to see what controls the transient association of KOR1 with the CSC.

In conclusion, we demonstrated here that KOR1 is an additional component of the CSC, that this interaction may be transient, and that KOR1 plays a role in the synthesis of cellulose but also in the intracellular trafficking of the CSC. We are currently investigating how this transient interaction and the intracellular trafficking are regulated and how *kor1* mutations affect the microfibril structure.

MATERIALS AND METHODS

Plant Material and in Vitro Growth Conditions

The GFP-CESA3 line was described previously (Desprez et al., 2007). *Arabidopsis* (*Arabidopsis thaliana*) plants were grown in the dark as described (Refrégier et al., 2004). For imaging, seedlings were cultured in chambers as described (Chan et al., 2007).

Cotton (*Gossypium hirsutum* 'Coker 310') plants were grown in the greenhouse (30°C during the day and 22°C at night; 50% hygrometry; light, 100 $\mu\text{mol m}^{-2} \text{s}^{-1}$). Flowers were tagged on the day of anthesis, and bolls were harvested at different days after anthesis. Fibers were separated from ovules and stored frozen.

Isolation of Crude Microsomal Membranes

Between 1 and 3 g of plant material (frozen fibers or *Arabidopsis* seedlings) was blended in homogenization buffer (250 mM Suc, 70 mM Tris-HCl, pH 8, 10% [v/v] glycerol, 3 mM Na₂EDTA, 4 mM dithiothreitol, 1.5% [v/w] polyvinylpyrrolidone, and 1% [v/v] protease inhibitor cocktail [Sigma P9599]). The homogenate was centrifuged for 15 min at 15,000g at 4°C. The resulting supernatant was filtered through Miracloth (Calbiochem). The filtrate was centrifuged for 1 h at 100,000g at 4°C. The pellet was resuspended in 150 mM NaCl, 100 mM Tris-HCl, pH 7.4, 1 mM EDTA, and 0.5% (w/v) Triton X-100 and stored at -80°C.

Gel Filtration Analysis

Protein extract was fractionated through a Superdex 200 10/300 GL gel filtration column (GE Healthcare) with 150 mM NaCl, 100 mM Tris-HCl, pH 7.4, 1 mM EDTA, and 0.1% (w/v) Triton X-100 S200 column buffer. The flow rate was 0.5 mL min⁻¹. Fractions (0.5 mL) were collected and precipitated with 4 volumes of acetone at -20°C overnight. Acetone was removed after a centrifugation of 30 min at 13,000g, and the pellets were resuspended in Laemmli buffer. The column was calibrated with gel filtration chromatography standards (Bio-Rad; thyroglobulin, 670 kD; bovine γ -globulin, 158 kD; chicken ovalbumin, 44 kD; equine myoglobin, 17 kD; and vitamin B12, 1.35 kD).

Denaturing Gel Electrophoresis and Immunoblotting

Proteins precipitated from the chromatography fractions were solubilized in Laemmli buffer and loaded on 8% (w/v) SDS-PAGE gels, blotted onto nitrocellulose membranes, and immunodetected with specific rabbit polyclonal antibodies against the N-terminal domain of KOR1 (α NKOR) or CESA1 (α CESA1) used at a 1:1,000 dilution. Secondary goat anti-rabbit horseradish peroxidase-conjugated antibody was purchased from Santa Cruz Biotechnology, and the chemiluminescence detection was performed using Clarity Western ECL substrate (Bio-Rad) and LAS-4000 luminescence image analyzer (Fujifilm).

Plant Expression Vectors

Constructs were made by using Gateway cloning technology (Invitrogen). A 1.3-kb fragment of the *KOR1* gene was amplified by PCR with specific primers (5'-CAAAGAAATACGGTCACATA-3' and 5'-TGATGATGCTCTCTGATAAAGC-3') and cloned into the *Hind*III-*Xba*I site of the pGWB6 vector after removal of the *35S* promoter. An LR reaction was performed to obtain the promoter *KOR1::GFP-KOR1* construct (GFP-KOR1). A 1.16-kb fragment of the *CESA1* promoter upstream of the initiation codon was amplified by PCR with specific primers containing *Hind*III and *Xba*I restriction sites (Miart et al., 2014) and cloned into the *Hind*III-blunted *Xba*I site of the pGWB2 vector. An *Xba*I fragment-mCherry fragment was then introduced in the pGWB2 vector. The CDNA of *CESA1* was amplified using specific primers (Miart et al., 2014), and Gateway reactions were performed to obtain the promoter *CESA1*-mCherry-*CESA1* construct (mCherry-*CESA1*).

The final expression vectors were electroporated in *Agrobacterium tumefaciens*. The GFP-KOR1 construct was introduced into *kor1-1* and *lit* mutants. mCherry-*CESA1* was introduced into the *cesa1^{tsu1-10}* mutant. Primary transformants were selected on hygromycin, and F2 progeny were used for visualization of the fluorescent protein.

BiFC constructs were described previously (Desprez et al., 2007), except the one concerning the *KOR1* gene. The *KOR1* version was amplified from the

complementary DNA KOR1 by PCR with specific primers (Table I). The BiFC construct was obtained by Gateway recombination.

Production of Transgenic Lines

Pollen from GFP-CESA3-expressing plants in the *cesa3^{ec5}* background or from GFP-KOR1-expressing plants was used to fertilize plants expressing monomeric red fluorescent protein-vacuolar H-ATP synthase isoform a1 (Dettmer et al., 2006), mCherry-RabA1g (Geldner et al., 2009), mCherry-Rab-GTP synthase G3c (Geldner et al., 2009), and mCherry-TUA6. Pollen from GFP-KOR1-expressing plants in the *kor1-1* background was used to fertilize plants expressing mCherry-CESA1. F1 seeds were collected and amplified. F2 seedlings were screened by PCR for the presence of both markers and the respective mutations. F3 selected seedlings were used for imaging GFP-CESA3 in wild-type plants.

Constructs for the MbYTH System

The constructs for the MbYTH system concerning the secondary CESAs were described previously (Timmers et al., 2009). The full-length complementary DNAs were obtained from the Riken Bioresource Center (Seki et al., 1998, 2002): AtCESA1 (RAFL09-89-G08), AtCESA3 (RAFL05-19-M03), AtCESA6 (RAFL05-02-P19), and AtKOR1 (RAFL05-02-G06). Restriction sites were generated by PCR with specific primers (Table I). The resulting PCR products were digested and ligated in the pTFB1 vector (bait plasmid) or the pADSL-Nx vector (prey plasmid; Dualsystems Biotech). The sequences of the inserts were confirmed by Sanger sequence analysis.

MbYTH Screen

The bait and prey constructs were cotransformed into the yeast (*Saccharomyces cerevisiae*) strain NMY51 (Dualsystems Biotech) according to the provided transformation procedure (DUAL Membrane Kit 1). The yeast, containing both plasmids, was plated onto synthetic medium lacking Leu and Trp and grown at 30°C for 3 d. To quantify the interactions between different preys, 100 colonies of each combination were spotted onto selection medium containing the appropriate amount of 3-ammonium-triazole and grown at 30°C for 3 d. The number of spots grown was then counted. Detection of β -galactosidase activity was performed with the filter-lift assay (Breedon and Nasmyth, 1985).

BiFC Screen

Leaves of 3-week-old *Nicotiana benthamiana* plants were transformed by infiltration as described (Voinnet et al., 2003). YFP fluorescence was detected 3 d after infiltration by using the 514-nm laser line of an SP2 AOBS confocal laser scanning microscope (Leica) equipped with an argon laser. To check the YFP reconstitution, spectral analysis was performed with the 496-nm laser line. The fluorescence with all constructs was detected at the same photomultiplier tube settings (760), except for the negative interactions, for which the photomultiplier tube was increased to 880.

Drug Treatments

Treatments for live-cell imaging were described previously (Crowell et al., 2009). Treatments were performed with 7 μ M oryzalin (Sigma) for 6 or 10 h or with 5 nM CGA (Bayer CropScience) for 3 h. Hypocotyl cells were stained with 50 μ M FM4-64 (Molecular Probes).

Spinning-Disk Analysis and Image Analysis

Spinning-disk analysis and image analysis were performed as described (Crowell et al., 2009). Hypocotyls of 3-d-old etiolated seedlings were analyzed on an Axiovert 200M microscope (Zeiss) equipped with a Yokogawa CSU22 spinning-disk Zeiss 100/1.4 numerical aperture oil objective and the Andor EMCCD iXon DU 895 camera (Plateforme d'Imagerie Dynamique, Institut Pasteur). GFP was excited at 488 nm by a diode-pumped solid-state laser, and fluorescence emission was collected through a 505/555-nm band-pass filter (Semrock). A 561-nm diode-pumped solid-state laser was used for the excitation of mCherry, and emission was collected using a band-pass 598- to 660-nm filter. GFP-KOR1 and GFP-CESA3 velocities were quantified by using the

manual tracking plugin (Fabrice Cordelières) in ImageJ (W. Rasban, National Institutes of Health). Particle density and colocalization analysis were performed after preprocessing using the ImageJ PureDenoise plugin (Luisier et al., 2009). A TopHat transformation (Serra, 1982) was used to extract circular signal from the background. Pearson's coefficients of colocalization were computed on TopHat-transformed dual-channel images using JACoP version 2.0 (Bolte and Cordelières, 2006).

Laser Scanning Confocal Microscopy

Images were collected with a spectral SP2 AOBS confocal microscope (Leica Microsystems) equipped with an argon laser. GFP and FM4-64 were detected using the laser line 488 nm.

Supplemental Data

The following materials are available in the online version of this article.

Supplemental Figure S1. Analysis of GhKOR during cotton fiber development.

Supplemental Figure S2. Complementation of the short-hypocotyl phenotype of *kor1-1* by GFP-KOR1 expressed from its endogenous promoter.

Supplemental Figure S3. GFP-KOR1 accumulates in a heterogenous population of organelles in epidermal cells of etiolated Arabidopsis hypocotyls.

Supplemental Figure S4. GFP-KOR1 trajectories at the plasma membrane are developmentally regulated and overlap with those of GFP-CESA3 and GFP-TUA6.

Supplemental Figure S5. Complementation of the short-hypocotyl phenotype of *cesa1^{tsu1-10}* by mCherry-CESA1 expressed from its endogenous promoter.

Supplemental Movie S1. GFP-KOR1 particles migrate at the plasma membrane.

Supplemental Movie S2. GFP-KOR1 and mCherry-CESA1 trajectories overlap.

Received April 11, 2014; accepted June 12, 2014; published June 19, 2014.

LITERATURE CITED

- Bolte S, Cordelières FP** (2006) A guided tour into subcellular colocalization analysis in light microscopy. *J Microsc* **224**: 213–232
- Bolte S, Talbot C, Boutte Y, Catrice O, Read ND, Satiat-Jeuemaitre B** (2004) FM-dyes as experimental probes for dissecting vesicle trafficking in living plant cells. *J Microsc* **214**: 159–173
- Breedon L, Nasmyth K** (1985) Regulation of the yeast HO gene. *Cold Spring Harb Symp Quant Biol* **50**: 643–650
- Brummell DA, Catala C, Lashbrook CC, Bennett AB** (1997) A membrane-anchored E-type endo-1,4-beta-glucanase is localized on Golgi and plasma membranes of higher plants. *Proc Natl Acad Sci USA* **94**: 4794–4799
- Chan J, Calder G, Fox S, Lloyd C** (2007) Cortical microtubule arrays undergo rotary movements in Arabidopsis hypocotyl epidermal cells. *Nat Cell Biol* **9**: 171–175
- Charrin S, Manié S, Thiele C, Billard M, Gerlier D, Boucheix C, Rubinstein E** (2003) A physical and functional link between cholesterol and tetraspanins. *Eur J Immunol* **33**: 2479–2489
- Crowell EF, Bischoff V, Desprez T, Rolland A, Stierhof YD, Schumacher K, Gonneau M, Höfte H, Vernhettes S** (2009) Pausing of Golgi bodies on microtubules regulates secretion of cellulose synthase complexes in *Arabidopsis*. *Plant Cell* **21**: 1141–1154
- Desprez T, Juraniec M, Crowell EF, Jouy H, Pochylova Z, Parcy F, Höfte H, Gonneau M, Vernhettes S** (2007) Organization of cellulose synthase complexes involved in primary cell wall synthesis in *Arabidopsis thaliana*. *Proc Natl Acad Sci USA* **104**: 15572–15577
- Dettmer J, Hong-Hermesdorf A, Stierhof YD, Schumacher K** (2006) Vacuolar H⁺-ATPase activity is required for endocytic and secretory trafficking in *Arabidopsis*. *Plant Cell* **18**: 715–730
- Diotallevi F** (2007) The physics of cellulose biosynthesis: polymerization and self-organization from plants to bacteria. PhD thesis. Wageningen

- University, Wageningen, The Netherlands <http://www.amolf.nl/publications/theses/diotallevi/diotallevi.html>
- Geldner N, Déneraud-Tendon V, Hyman DL, Mayer U, Stierhof YD, Chory J** (2009) Rapid, combinatorial analysis of membrane compartments in intact plants with a multicolor marker set. *Plant J* **59**: 169–178
- Gutierrez R, Lindeboom JJ, Paredez AR, Emons AM, Ehrhardt DW** (2009) Arabidopsis cortical microtubules position cellulose synthase delivery to the plasma membrane and interact with cellulose synthase trafficking compartments. *Nat Cell Biol* **11**: 797–806
- Haigler CH, Grimson MJ, Gervais J, Le Moigne N, Höfte H, Monasse B, Navard P** (2014) Molecular modeling and imaging of initial stages of cellulose fibril assembly: evidence for a disordered intermediate stage. *PLoS ONE* **9**: e93981
- Höfte H, Gonneau M, Vernhettes S** (2007). Biosynthesis of cellulose. In JP Kamerling, ed, *Comprehensive Glycoscience*. Elsevier, Miamisburg, OH, pp 737–763
- Lane DR, Wiedemeier A, Peng L, Höfte H, Vernhettes S, Desprez T, Hocart CH, Birch RJ, Baskin TI, Burn JE, et al** (2001) Temperature-sensitive alleles of *RSW2* link the KORRIGAN endo-1,4- β -glucanase to cellulose synthesis and cytokinesis in Arabidopsis. *Plant Physiol* **126**: 278–288
- Lei L, Li S, Bashline L, Gu Y** (2014) Dissecting the molecular mechanism underlying the intimate relationship between cellulose microfibrils and cortical microtubules. *Front Plant Sci* **5**: 90
- Luisier F, Vonesch C, Blu T, Unser M** (2009) Fast Haar-wavelet denoising of multidimensional fluorescence microscopy data. In Proceedings of the Sixth IEEE International Symposium on Biomedical Imaging: From Nano to Macro (ISBI '09), Boston, MA, pp 310–313
- Master ER, Rudsander UJ, Zhou W, Henriksson H, Divne C, Denman S, Wilson DB, Teeri TT** (2004) Recombinant expression and enzymatic characterization of PttCel9A, a KOR homologue from *Populus tremula* \times *tremuloides*. *Biochemistry* **43**: 10080–10089
- Meinert MC, Delmer DP** (1977) Changes in biochemical composition of the cell wall of the cotton fiber during development. *Plant Physiol* **59**: 1088–1097
- Miart F, Desprez T, Biot E, Morin H, Belcram K, Höfte H, Gonneau M, Vernhettes S** (2014) Spatio-temporal analysis of cellulose synthesis during cell plate formation in Arabidopsis. *Plant J* **77**: 71–84
- Mølhoj M, Pagant S, Höfte H** (2002) Towards understanding the role of membrane-bound endo-beta-1,4-glucanases in cellulose biosynthesis. *Plant Cell Physiol* **43**: 1399–1406
- Mølhoj M, Ulvskov P, Dal Degan F** (2001) Characterization of a functional soluble form of a *Brassica napus* membrane-anchored endo-1,4- β -glucanase heterologously expressed in *Pichia pastoris*. *Plant Physiol* **127**: 674–684
- Morgan JL, Strumillo J, Zimmer J** (2013) Crystallographic snapshot of cellulose synthesis and membrane translocation. *Nature* **493**: 181–186
- Nakai T, Sugano Y, Shoda M, Sakakibara H, Oiwa K, Tuzi S, Imai T, Sugiyama J, Takeuchi M, Yamauchi D, et al** (2013) Formation of highly twisted ribbons in a carboxymethylcellulase gene-disrupted strain of a cellulose-producing bacterium. *J Bacteriol* **195**: 958–964
- Newman RH, Hill SJ, Harris PJ** (2013) Wide-angle x-ray scattering and solid-state nuclear magnetic resonance data combined to test models for cellulose microfibrils in mung bean cell walls. *Plant Physiol* **163**: 1558–1567
- Nicol F, His I, Jauneau A, Vernhettes S, Canut H, Höfte H** (1998) A plasma membrane-bound putative endo-1,4-beta-D-glucanase is required for normal wall assembly and cell elongation in Arabidopsis. *EMBO J* **17**: 5563–5576
- Paredez AR, Persson S, Ehrhardt DW, Somerville CR** (2008) Genetic evidence that cellulose synthase activity influences microtubule cortical array organization. *Plant Physiol* **147**: 1723–1734
- Paredez AR, Somerville CR, Ehrhardt DW** (2006) Visualization of cellulose synthase demonstrates functional association with microtubules. *Science* **312**: 1491–1495
- Peng L, Hocart CH, Redmond JW, Williamson RE** (2000) Fractionation of carbohydrates in Arabidopsis root cell walls shows that three radial swelling loci are specifically involved in cellulose production. *Planta* **211**: 406–414
- Peng L, Kawagoe Y, Hogan P, Delmer D** (2002) Sitosterol-beta-glucoside as primer for cellulose synthesis in plants. *Science* **295**: 147–150
- Persson S, Paredez A, Carroll A, Palsdottir H, Doblin M, Poindexter P, Khitrov N, Auer M, Somerville CR** (2007) Genetic evidence for three unique components in primary cell-wall cellulose synthase complexes in Arabidopsis. *Proc Natl Acad Sci USA* **104**: 15566–15571
- Read SM, Bacic T** (2002) Prime time for cellulose. *Science* **295**: 59–60
- Refrégier G, Pelletier S, Jaillard D, Höfte H** (2004) Interaction between wall deposition and cell elongation in dark-grown hypocotyl cells in Arabidopsis. *Plant Physiol* **135**: 959–968
- Robert S, Bichet A, Grandjean O, Kierzkowski D, Satiat-Jeunemaitre B, Pelletier S, Hauser MT, Höfte H, Vernhettes S** (2005) An Arabidopsis endo-1,4- β -D-glucanase involved in cellulose synthesis undergoes regulated intracellular cycling. *Plant Cell* **17**: 3378–3389
- Robert S, Mouille G, Höfte H** (2004) The mechanism and regulation of cellulose synthesis in primary walls: lessons from cellulose-deficient Arabidopsis mutants. *Cellulose* **11**: 351–364
- Sato S, Kato T, Kakegawa K, Ishii T, Liu YG, Awano T, Takabe K, Nishiyama Y, Kuga S, Sato S, et al** (2001) Role of the putative membrane-bound endo-1,4-beta-glucanase KORRIGAN in cell elongation and cellulose synthesis in Arabidopsis thaliana. *Plant Cell Physiol* **42**: 251–263
- Seki M, Carninci P, Nishiyama Y, Hayashizaki Y, Shinozaki K** (1998) High-efficiency cloning of Arabidopsis full-length cDNA by biotinylated CAP trapper. *Plant J* **15**: 707–720
- Seki M, Narusaka M, Kamiya A, Ishida J, Satou M, Sakurai T, Nakajima M, Enju A, Akiyama K, Oono Y, et al** (2002) Functional annotation of a full-length Arabidopsis cDNA collection. *Science* **296**: 141–145
- Serra J** (1982) *Image Analysis and Mathematical Morphology*. Academic Press, London
- Somerville C** (2006) Cellulose synthesis in higher plants. *Annu Rev Cell Dev Biol* **22**: 53–78
- Szyjanowicz PM, McKinnon I, Taylor NG, Gardiner J, Jarvis MC, Turner SR** (2004) The irregular xylem 2 mutant is an allele of korrgan that affects the secondary cell wall of Arabidopsis thaliana. *Plant J* **37**: 730–740
- Taylor NG, Howells RM, Huttly AK, Vickers K, Turner SR** (2003) Interactions among three distinct CesA proteins essential for cellulose synthesis. *Proc Natl Acad Sci USA* **100**: 1450–1455
- Taylor NG, Laurie S, Turner SR** (2000) Multiple cellulose synthase catalytic subunits are required for cellulose synthesis in Arabidopsis. *Plant Cell* **12**: 2529–2540
- Taylor NG, Scheible WR, Cutler S, Somerville CR, Turner SR** (1999) The *irregular xylem3* locus of Arabidopsis encodes a cellulose synthase required for secondary cell wall synthesis. *Plant Cell* **11**: 769–780
- Timmers J, Vernhettes S, Desprez T, Vincken JP, Visser RG, Trindade LM** (2009) Interactions between membrane-bound cellulose synthases involved in the synthesis of the secondary cell wall. *FEBS Lett* **583**: 978–982
- Voinnet O, Rivas S, Mestre P, Baulcombe D** (2003) An enhanced transient expression system in plants based on suppression of gene silencing by the p19 protein of tomato bushy stunt virus. *Plant J* **33**: 949–956
- Zuo J, Niu QW, Nishizawa N, Wu Y, Kost B, Chua NH** (2000) KORRIGAN, an Arabidopsis endo-1,4- β -glucanase, localizes to the cell plate by polarized targeting and is essential for cytokinesis. *Plant Cell* **12**: 1137–1152